Electrically Bistable Properties of Layer-by-Layer Assembled Multilayers Based on Protein Nanoparticles

Yongmin Ko,[†] Younghoon Kim,[‡] Hyunhee Baek,[‡] and Jinhan Cho[‡,*]

[†]School of Advanced Materials Engineering, Kookmin University, Jeongneung-dong, Seongbuk-gu, Seoul 136-702, Korea and, [‡]Department of Chemical and Biological Engineering, Korea University, Anam-dong, Seongbuk-gu, Seoul 136-713, Korea

ABSTRACT

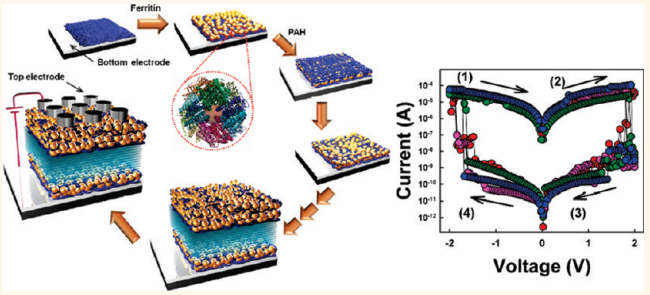

Electrochemical properties of redox proteins, which can cause the reversible changes in the resistance according to their redox reactions in solution, are of the fundamental and practical importance in bioelectrochemical applications. These redox properties often depend on the chemical activity of transition metal ions as cofactors within the active sites of proteins. Here, we demonstrate for the first time that the reversible resistance changes in dried protein films based on ferritin nanoparticles can be caused by the externally applied voltage as a result of charge trap/release of Fe^{III}/Fe^{II} redox couples. We also show that one ferritin nanoparticle of about 12 nm size can be operated as a nanoscale-memory device, and furthermore the layer-by-layer assembled protein multilayer devices can be extended to bioinspired electronics with adjustable memory performance *via* molecular level manipulation.

KEYWORDS: layer-by-layer assembly · multilayers · ferritin · redox · nonvolatile memory

Ferritin is one of the most widely used biomolecules for the preparation of bioinspired nanomaterials.[1−3] Ferritin is a highly stable iron-storage protein with an outer diameter of ∼12 nm and a shell thickness of ∼2 nm. It is produced by almost all living organisms including bacteria, algae, higher plants, and animals and acts as a buffer against iron deficiency and iron overload in organisms. The ∼8-nm-diameter-sized cavity of ferritin has been used as a nanoreactor, and its structural stability has allowed ferritin to be used for the synthesis of various nanostructured materials *via* ion exchange and pyrolysis.[4−7] Although extensive studies involving ferritin have been published, relatively little effort has been put into investigating the electrical properties of ferritin or the design of ferritin-based bioelectronics. Recently, Xu *et al*. has reported measurement of the direct electrical conductivity of a ferritin layer in dry form,[8] as opposed to the more typical measurements of the electrochemical redox reaction of ferritin in aqueous solution using cyclic voltammetry. We have focused on the possibility that a high density of Fe ions within dried ferritin films may have resistance-switching properties as a consequence of the charge trap/release of Fe^{III}/Fe^{II} pairs induced by externally applied voltage. This possibility is very significant because it would allow a variety of proteins containing Fe^{III}/Fe^{II} redox couples as well as ferritin to be employed as an electrically active material for the resistive-switching-based nonvolatile memory devices applicable to mobile electronics.

To date, a variety of synthesized organic nonvolatile memory devices that exhibit excellent performance have been introduced; in many cases, they have exhibited write-once/read-many-times (WORM)-type memory behavior without rewritable ON and OFF states.[9,10] Recently, it was reported that organic memory devices with reversible ON and OFF states as well as high memory performance could be prepared using a spin-coated insulating organic matrix that contains charge trap elements, such as graphene or inorganic nanoparticles.[11,12]

In this study, we report for the first time that the one protein nanoparticle for nanoscale devices as well as protein-based multilayers can be used as a nonvolatile memory device and that its switching behavior originates from redox sites (*i.e*., ferrihydrite core) within the protein. Furthermore, it is demonstrated that the memory performance of protein multilayers can be

* Address correspondence to jinhan71@korea.ac.kr.

Received for review September 26, 2011 and accepted November 17, 2011.

Published online November 17, 2011
10.1021/nn2036939

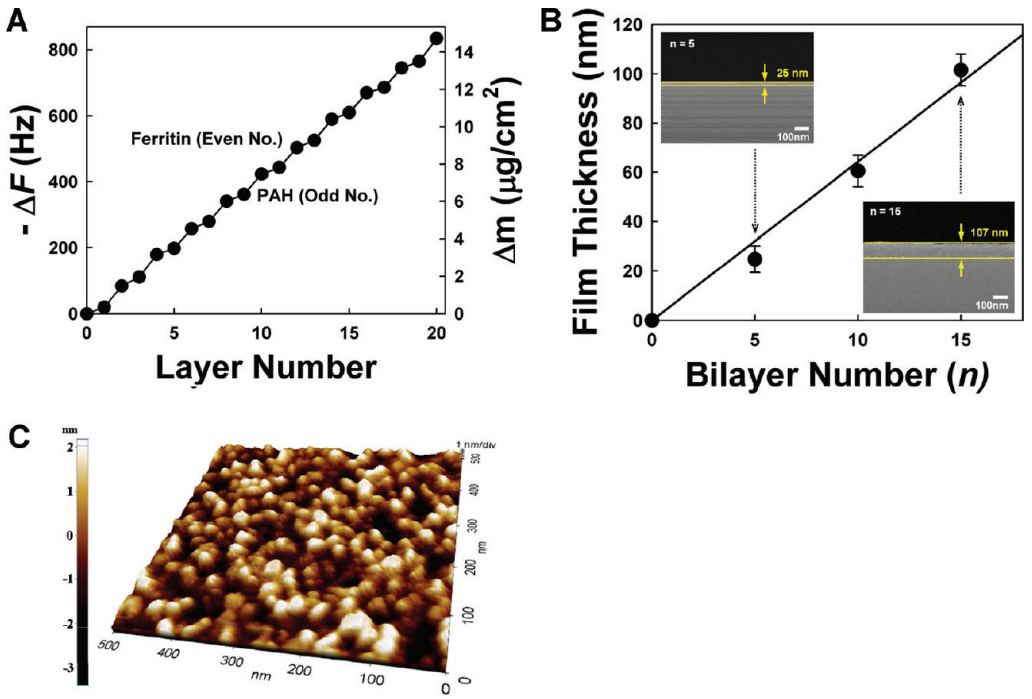

Figure 1. (A) QCM data of PAH/ferritin multilayers as a function of the layer number. (B) Film thicknesses of (PAH/ferritin)$_{n=5,10,\ \text{and}\ 15}$ multilayers measured from cross-sectional SEM images after drying under vacuum. The insets show cross-sectional SEM images of 5 and 15 bilayered films. (C) 3D AFM images of (PAH/ferritin)$_{15}$ multilayers. Root-mean-square surface roughness was measured to be about 1.2 nm.

significantly improved by layer-by-layer (LbL) multilayer design. For this investigation, multilayer films composed of anionic ferritin and cationic poly(allylamine hydrochloride) (PAH) were deposited onto Pt-coated substrates using the electrostatic LbL assembly method.[13−23] Although a variety of methods (*i.e.*, vacuum deposition[24] sol−gel coating,[25] and spin-coating[9−12,26]) for preparing dry memory devices with ON/OFF current ratio above ~10^3 and low operating voltages of about 3 V have been introduced to date, a LbL assembly method based on a solution dipping process is quite useful for preparing electrical films with tailored electrical properties and layer thickness as well as various functional components on substrates of different sizes and shape. The importance of our work lies in the fact that electrochemical characteristic of proteins can be extended to nonvolatile memory properties, and furthermore protein films can be designed as high-performance memory device *via* LbL assembly manipulation. Therefore, we believe that our approach using LbL assembly can provide a basis for the development of a new field of study such as nonvolatile memory related to a variety of protein-based nanomaterials as well as ferritin.

RESULTS AND DISCUSSION

The isoelectric point of ferritin lies in the pH range 4.5−4.8;[6] therefore, ferritin exhibits an overall positive charge at pH < 4.5 and an overall negative charge at pH >5. In addition, the pK_a (*i.e.*, the pH value at which 50% of a polymer's functional groups are ionized) of PAH in bulk solution is approximately 9.[27] These phenomena indicate that ferritin and PAH can be used as anionic and cationic species at pH 9, respectively. On the basis of this electrostatic interaction, the quantitative growth of multilayers was monitored by quartz crystal microgravimetry (QCM). Figure 1A shows the frequency changes, $-\Delta F$, and the mass changes of adsorbed PAH and ferritin that result from an increasing number of layers. The mass changes were calculated from the frequency changes (see Methods). These QCM frequency (or mass) changes indicate that regular multilayer film growth occurs when PAH and ferritin are LbL-assembled from the deposition solutions. The alternating deposition of PAH and ferritin results in $-\Delta F$ of 21 ± 5 (Δm of ~366 ng·cm^{-2}) and 63 ± 4 Hz (Δm of ~1106 ng·cm^{-2}), respectively, per layer. The thickness of (PAH/ferritin)$_n$ multilayers was regularly increased from 0 to 107 nm with increasing bilayer number (n) from 0 to 15 (Figure 1B). In this case, the measured film thicknesses did not coincide with ideal film thickness considering ~12 nm-sized ferritin with about 1.20 g·cm^{-3} adsorbed PAH layer thickness and bilayer number because the insufficient surface coverage (~43%) of ferritin is caused by the electrostatic repulsion between the same charged ones.[28,29] This insufficient surface coverage was also confirmed by AFM imaging of (PAH/ferritin)$_{15}$ multilayers with a root-mean-square surface roughness of about 1.2 nm (Figure 1C).

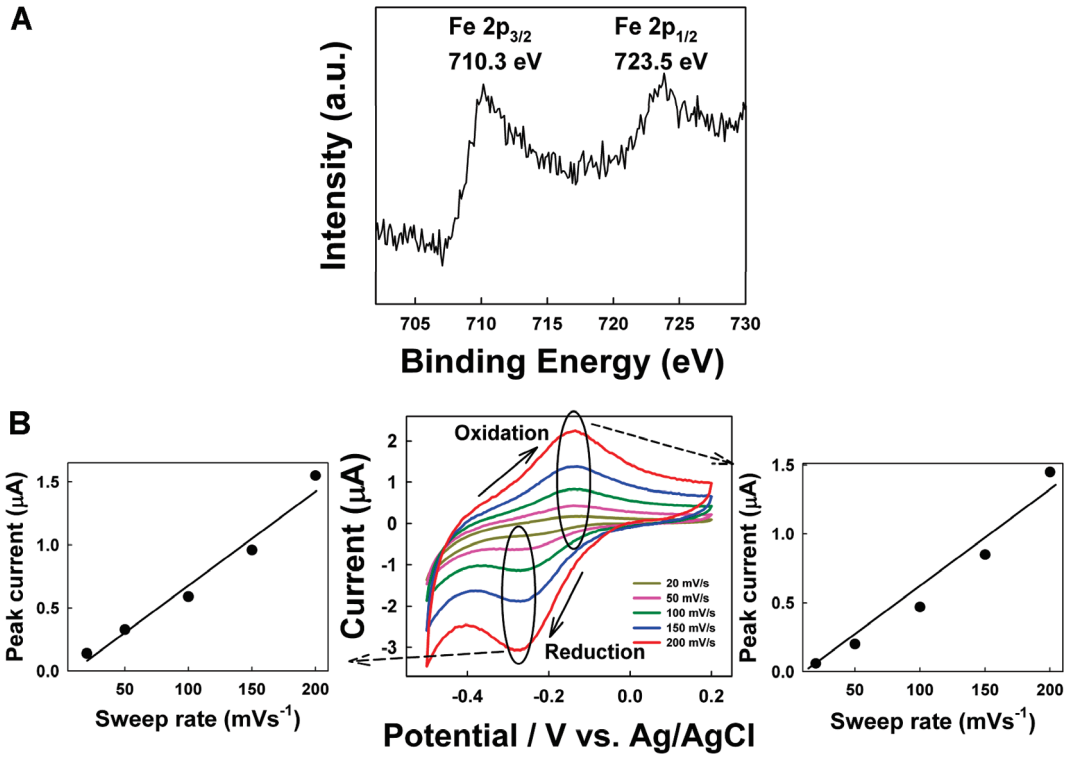

Figure 2. (A) XPS spectrum of PAH/ferritin multilayers. (B) Cyclic voltammograms from PAH/ferritin multilayer-coated indium tin oxide electrodes with an electrode area of 0.5 cm^2 in phosphate buffer solutions at pH 7 (potential sweep rates: 200, 150, 100, 50, and 20 $mV \cdot s^{-1}$), and plots of anodic and cathodic peak currents *vs* potential sweep rates.

As confirmed from the X-ray photoelectron spectroscopy (XPS) pattern of PAH/ferritin multilayers, the spectral shape and binding energies of the significant peaks of Fe $2p_{3/2}$ (710.3 eV) and Fe $2p_{1/2}$ (723.5 eV) were caused by the presence of ferrihydrite phosphate within the core of ferritin (Figure 2A).[30,31] Additionally, these Fe ions give rise to the redox reaction of ferritin. As shown in Figure 2B, the formed PAH/ferritin multilayers displayed typical electrochemical redox behavior that originated from ferritin in pH 7.0 phosphate buffer solution (PBS); increased scan rates resulted in higher intensities of the redox peaks (*i.e.*, the oxidation peak at −0.15 V and the reduction peak at −0.27 V). During the cyclic voltammetry (CV) scans, Fe^{III} atoms, which compose ferrihydrite cores, were reduced to Fe^{II} during negative potential sweeps, and Fe^{II} was oxidized to Fe^{III} during positive potential sweeps. The redox peak currents increase linearly with scan rate, indicating that the electrochemical response is governed by a charge-transfer mechanism.[32,33] Additionally, the iron uptake and release mechanism is caused by a Fe^{III}/Fe^{II} redox reaction in solution state because the solubility of Fe^{II} is higher than that of Fe^{III}.[34,35] As a result, ferritin multilayers with electrochemical redox reactions were deposited onto substrates, and the layer thickness and amount of adsorbed ferritin were precisely controlled.

We prepared nonvolatile memory devices composed of $(PAH/ferritin)_n$ multilayers deposited onto Pt-coated Si substrates and Ag top electrodes with diameters of 100 μm deposited onto the multilayer films as shown in Scheme 1. In this case, PAH/ferritin multilayer films were sufficiently dried under vacuum to completely remove the residual water before the deposition of Ag electrodes. Our strategy is based on the possibility that the reversible resistance change of a ferritin multilayer device can be controlled by the charge trapping and release of Fe^{III}/Fe^{II} couples under an externally applied voltage in an air environment.

The electrical measurements of nonvolatile memory cells were performed using applied voltage in an air atmosphere. In a typical bipolar switching measurement that depends on voltage polarity, voltage sweeps from −2.0 V to +2.0 V and back to −2.0 V were applied with the current limited to 100 mA. The high-current state (ON state) formed after the initial electroforming stage (for a conductive path within multilayers) was suddenly converted to a low-current state (RESET process for OFF state) at +1.5 V when the reverse voltage polarity was applied to the $(PAH/ferritin)_{n=5,10,15}$ multilayered devices. This low-current state (OFF state) was maintained from +2.0 V to −1.5 V and then converted to the high-current state at −1.5 V (SET process for ON state). In addition, an increased number of bilayers (*i.e.*, increased multilayer thickness) significantly lowered the OFF current level because the increased film thickness decreased the electric field level (Figure 3A). As a result, the ON/OFF current ratio of these devices was increased to $\sim 10^3$.

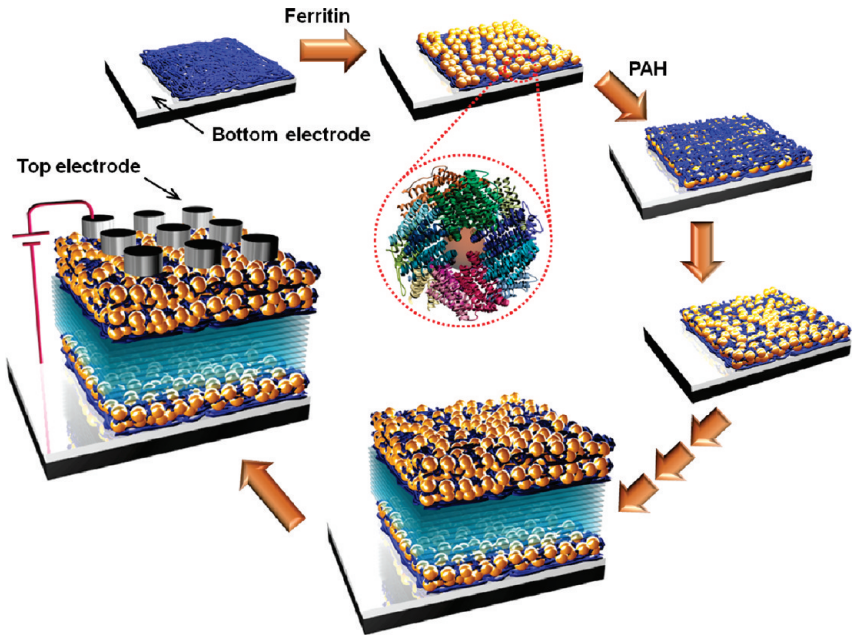

Scheme 1. Schematics for the Setup of PAH/Ferritin Multilayer-Based Nonvolatile Memory Devices

To further investigate the stability of the resistive switching properties, cycling and retention time tests of 15 bilayered PAH/ferritin film devices were performed to determine their electrical stability in the ON and OFF states using a reading voltage of +0.1 V (Figure 3B and C). In these cases, the ON and OFF states were kept continuously stable during the repeated cycling tests of approximately 300 cycles with a fast switching speed of 100 ns and a test period of 10^4 s in air. These reversible switching properties were still maintained after one year (see Supporting Information, Figure S1). Recently, solid electrolytes or transition metal oxides sandwiched between an electrochemically active Ag and an inert electrode have been reported to exhibit resistive-switching behavior because of an electrochemical redox reaction based on the high mobility of Ag ions.[36−38] Although Ag electrodes were used as the top electrodes in our system, a similar switching behavior was also observed with electrochemically inert tungsten (W) top electrodes. That is, the $(PAH/ferritin)_{15}$ multilayers sandwiched between Pt (bottom) and W (top) electrodes exhibited an ON/OFF ratio greater than 10^3, which was similar to that measured from multilayer devices with a Ag top electrode. Additionally, the conventional polyelectrolyte multilayers composed of cationic PAH and anionic poly(acrylic acid) (PAA) without charge trap sites showed insulating characteristics without any switching memory (see Supporting Information, Figure S2). Furthermore, the apoferritin-based multilayers (*i.e.*, $(PAH/apoferritin)_{15}$) without Fe^{III}/Fe^{II} redox couples did not exhibit the ON current state shown in the $(PAH/ferritin)_{15}$ film, and their conductivity level was also lower than the OFF current level of the $(PAH/ferritin)_{15}$ film (see Supporting Information, Figure S3).[8] These results evidently show that the films containing no charge tap sites do not have reversible resistive switching behavior, and furthermore the metal ion diffusion of metal electrodes into the films has no meaningful effect on the resistive switching behavior.

Although a variety of switching mechanisms for resistive-switching memory devices have been reported,[19,39−42] the memory effect in these devices may be due to charge storage (low conductivity) and release (high conductivity) within the charge-trap sites such as the ferrihydrite core.[23,43−45] First, the negative voltage sweep of devices from −2.0 to 0 V releases the electrons from the redox sites (*i.e.*, region (1) in Figure 3A) and induces a highly conductive state. This ON state is maintained until the electrons are partially injected into the redox sites (*i.e.*, (2)), and they are trapped in redox sites until the voltage polarity is reversed (*i.e.*, (2) → (3)). However, after the reversal of the voltage polarity, the conductive paths for electrons in the PAH/ferritin multilayers are broken down, which resulted in a decrease in conductivity that corresponds to the RESET process (*i.e.*, switching from the high-current to the low-current state). The OFF state is maintained to approximately −1.5 V (*i.e.*, region (4)). However, an increase in the external electric field to release the trapped electrons from within the redox sites (*i.e.*, region (4)) is thought to sharply increase the conductivity at the SET voltage (*i.e.*, $V_{SET} \approx -1.5$ V for the SET process).

The conduction mechanism of the PAH/ferritin multilayers was further investigated using the nonlinear *I*−*V* characteristics plotted on a log−log scale for the negative voltage sweep (*i.e.*, from region (4) to region

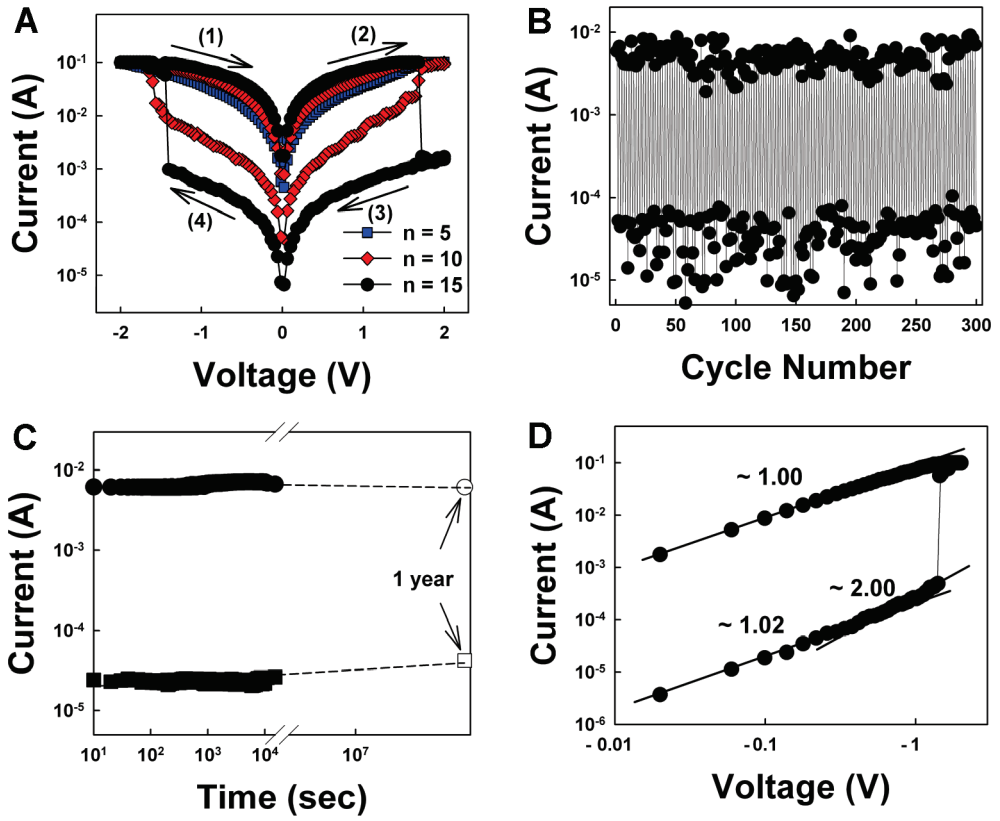

Figure 3. (A) *I*–*V* curves of (PAH/ferritin)$_n$ multilayer devices with bilayer number (n) from n = 5 to 15. (B) Cycling and (C) retention time tests of a 15-bilayered device measured at a switching speed of 100 ns at a reading voltage of 0.1 V. Retention time stability after 1 year is expected from the slope of ON and OFF current state. (D) Linear fitting for the *I*–*V* curve of a 15-bilayered device plotted on a log–log scale for the SET process during a negative voltage sweep.

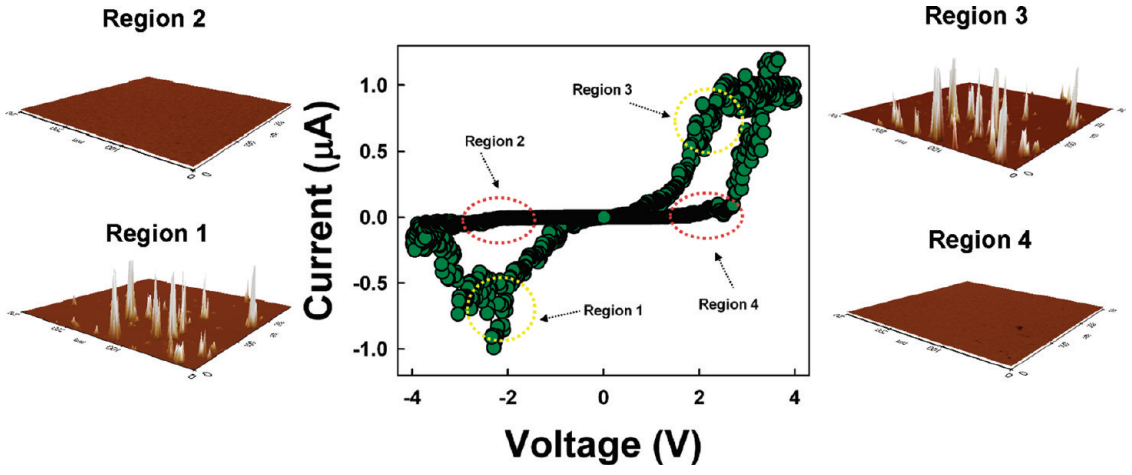

Figure 4. *I*–*V* curve and CS-AFM images of (PAH/ferritin)$_3$ multilayers in the ON (region 3) and OFF state (region 4) during positive voltage sweep, and the ON (region 1) and OFF (region 2) state during negative voltage sweep, respectively. CS-AFM images of multilayer devices were measured from the respective regions in the *I*–*V* curve of a (PAH/ferritin)$_3$ multilayer device. The formation of conductive filamentary paths was confirmed by CS-AFM characterizations. In this case, an electrochemically inert Pt tip was used as a top electrode instead of the Ag electrode. The formation and rupture of the randomly distributed paths were observed after "SET" processes (*i.e.*, switching from low-current (OFF) to high-current (ON) state) and "RESET" (*i.e.*, switching from high-current (ON) to low-current (OFF) state).

(1) in Figure 3A). Figure 3D shows that the *I*–*V* relationship in the ON state of PAH/ferritin films clearly exhibited ohmic conduction behavior with a slope of 1.02. In this case, ON current might flow through a local conduction path, such as a metallic filament acting as a resistor with low resistivity. On the other hand, the fitting results for the OFF state showed a charge transport behavior similar to that of space-charge-limited

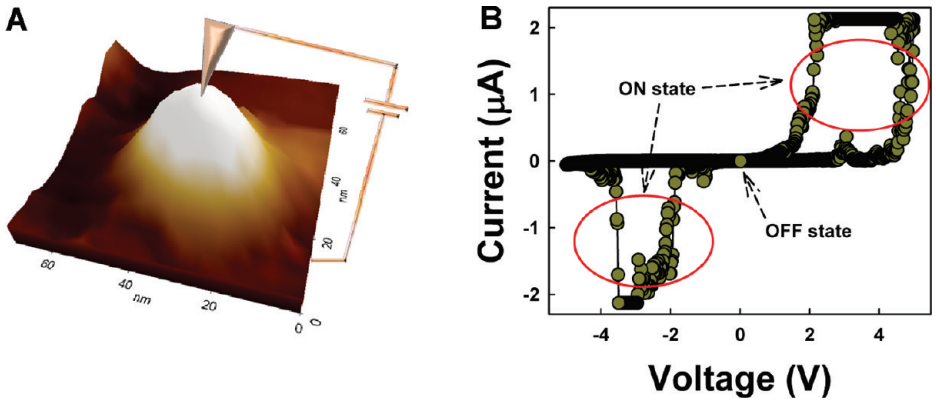

Figure 5. (A) Schematic and (B) *I*−*V* curve of one bare ferritin nanoparticle measured from CS-AFM with current compliance of 2.1 μA.

conduction (SCLC) with a trap model.[16,45,46] The SCLC model consists of an ohmic current region ($I \propto V$) because of thermally generated charge carriers, a Mott−Gurney law region (also known as Child's law in solids) ($I \propto V^2$), and a region of sharp current increase. These phenomena indicate that ferrihydrite cores of ferritin act as trap sites that capture electrons injected from electrode and that the electrons captured in the trap are easily emitted under a high electric field (*i.e.*, formation of local conductive path as a result of charge release). The different conduction behaviors in the ON and OFF states also suggest that the high conductivity in the ON-state device is a localized conducting effect rather than a homogeneously distributed one. The formation of localized conductive filamentary paths was also confirmed using current-sensing atomic force microscopy (CS-AFM) characterizations (Figure 4). For the CS-AFM measurement, a $(PAH/ferritin)_3$ multilayer film was deposited onto Pt-coated substrates, and then an electrochemically inert Pt CS-AFM tip with contact area of about 30 nm was used as a top electrode instead of a Ag electrode of 100 μm size. In this case, the formation and rupture of randomly distributed paths were observed in ON (*i.e,* region (1) and (3)) and OFF state (i.e., region (2) and (4)) measured from the *I*−*V* curve of three-bilayered PAH/ferritin films. Furthermore, the relatively low conductivity and high operating voltages shown in CS-AFM data compared to those in Figure 3A are mainly caused by tip size and an additional energy barrier between films and tip electrode.

That is, for the measurement of the memory cell shown in Figure 3A, the 100 μm-sized electrodes were used as a top electrode. On the other hand, the AFM tip electrode has an electrical point source with an extremely small contact area of about 20−30 nm, causing the increase of resistance. Furthermore, the surface interfacial contamination on conducting AFM surfaces may provide an additional energy barrier for the contact resistance. Therefore, the current level of ON and OFF states measured from the AFM tip electrode is relatively low compared to that from the large-size electrode of a memory cell. Additionally, considering that the electron transport in organic materials containing transition metal complexes is mainly caused by an electron-hopping process,[47] this conductive path is formed by electron hopping between charge trap sites. Furthermore, we investigated the possibility that one bare ferritin particle without any coated polyelectrolytes could operate as a nanoscale memory device (Figure 5A). For this investigation, ferritin-coated substrates were prepared onto a Pt-coated Si substrate using ferritin solution with an extremely diluted concentration of 1×10^{-6} mg·mL^{-1}. In this case, the nonvolatile memory properties of one ferritin particle in an area of 70×70 nm^2 was measured using the CS-AFM tip electrode with a current compliance of 2.1 μA. As shown in Figure 5B, one ferritin nanoparticle displayed an ON/OFF current ratio of $\sim 10^3$, inducing the typical bipolar switching behavior (see also Supporting Information, Figure S4).

To demonstrate the switching mechanism based on the trap and release of charges, nonvolatile memory properties have been investigated using kelvin force microscopy (KFM) (Figure 6A). First, a 12×12 μm^2 area of the multilayer film was scanned at +12 V to induce charge trapping. Next, an 8×8 μm^2 area was scanned at −12 V to induce charge release. The charge-trap operation was successively performed by scanning a 4.5×4.5 μm^2 area with a + 12 V bias. A −12 V bias was applied to a 1.5×1.5 μm^2 area for the charge release. In Figure 6A, the yellow region indicates the charge-trap state, and the dark region corresponds to the charge-release state. Consequently, the evident contrast changes of the KFM image obtained from charge trapping/releasing operations strongly support our hypothesis that the nonvolatile memory effects of our device originate from ferrihydrite of ferritin.

On the basis of these results, we have tried to improve the memory performance of ferritin multilayer devices by the further insertion of insulating layers of about 2 nm thickness between ferrtin layers (*i.e.*, $(PAH/ferritin/PAH/PAA)_{10}$). These films were thermally annealed at 150 °C to completely remove the residual water

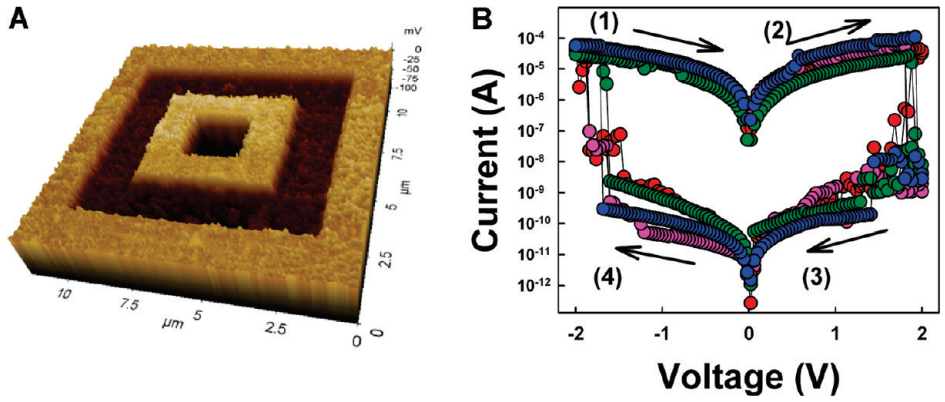

Figure 6. (A) 3D KFM image of PAH/ferritin multilayers for the charge-trap/release operations. (B) Repeated *I*−*V* curves of (PAH/ferritin/PAH/PAA)$_{10}$ multilayers.

with films. This LbL multilayer design effectively screened the leakage current (particularly, OFF current level) in ON and OFF current states, and as a result induced low power consumption (Figure 6B). In this case, the (PAH/ferritin/PAH/PAA)$_{10}$ multilayer device exhibited the higher ON/OFF current ratio of $\sim 10^6$ and the low current level of ON current level of 10^{-4} A and OFF current of 10^{-11}A at a reading voltage of −0.1 V than those of PAH/ferritin devices. The device performance shown in our approach was comparable to those of previously reported inorganic[25,37] or organic memory devices[9,46] with high memory performance. Considering that conventional vacuum deposition or spin-coating methods have much difficulty in modulating electrical properties *via* molecular level manipulation, our approach is very effective for preparing a high-performance memory device with a facile solution process.

CONCLUSIONS

We have demonstrated for the first time that LbL-assembled ferritin multilayers in a dry form exhibit the bistable electrical-switching behaviors that can be used to create nonvolatile memory under applied voltages. These phenomena were mainly caused by the charge trap/release of the Fe^{III}/Fe^{II} redox couples within ferritin. Additionally, because Fe ions within ferritin can be easily replaced by different kinds of transition metal ions using their ion exchanging properties, our approach can be applied to nonvolatile memory devices and thereby allows a variety of charge trap elements. In future publications, we will also show that a variety of proteins (*i.e,* catalase, myoglobin, or hemoglobin) as well as ferritin-containing Fe ions can display the resistive switching properties and their memory performance can be significantly improved by LbL assembly manipulation such as the insertion of insulating PEs. Therefore, we believe that our approach can be extended to bioinspired electronics requiring high performance *via* a versatile surface chemistry, *i.e,* LbL assembly process.

METHODS

Preparation of Multilayers. The concentration of ferritin (from equine spleen, Aldrich), apoferritin (from equine spleen, Aldrich), and PAH (M_w = 70 000, Aldrich) solutions used for all the experiments was 1 mg·mL^{-1}. The solution pH of ferritin and PAH was adjusted to 9. In this case, ferritin was used as an anionic component at pH 9, and on the other hand, PAH was used as cationic components at pH 9. Pt-coated Si substrates had an anionic surface by irradiating UV light. These substrates were first dipped for 10 min in the cationic PAH solution, washed twice by dipping in water for 1 min, and air-dried with a gentle stream of nitrogen. Anionic ferritin was subsequently deposited onto the PAH-coated substrates by using the same adsorption, washing, and drying procedures as described above. This process was repeated until the desired number of layers was deposited. The resultant multilayer films were sufficiently dried under vacuum conditions.

QCM Measurements. A QCM device (QCM200, SRS) was used to investigate the mass of material deposited after each adsorption step. The resonance frequency of the QCM electrodes was *ca.* 5 MHz. The adsorbed mass of PAH and ferritin, Δm, can be calculated from the change in QCM frequency, ΔF, according to the Sauerbrey equation: ΔF (Hz) = $-56.6\Delta m_A$, where Δm_A is the mass change per quartz crystal unit area in μg·cm^{-2}.

Fabrication of Resistive Switching Memory Devices. All the samples were prepared on Si substrates (2 cm × 2 cm) with a SiO_2 layer of about 100 nm thickness. A Ti layer of 20 nm thickness was then deposited on the substrates, and the bottom electrode (Pt) was subsequently deposited using a DC-magnetron sputtering system. The (PAH/ferritin)$_n$ multilayer films were then formed on the Pt-coated Si substrates. The resultant multilayer films were dried for 4 h under vacuum conditions. After completely removing residual moisture within the films, top electrodes with 100 μm diameter were deposited onto the nanocomposite films. To investigate the resistive switching behavior of LbL multilayered devices, the current−voltage (*I*−*V*) curves were measured by a semiconductor parametric analyzer (SPA, Agilent 4155B) in air environment. The pulsed voltage duration dependence of high- and low-current states was investigated using a semiconductor parametric analyzer (HP 4155A) and pulse generator (Agilent 81104A). In this case, the current compliance was limited to 100 mA in order to prevent total dielectric breakdown of the device from overcurrent. The high-current state (ON state) formed after the initial electroforming

process (*i.e.*, current-limited electric breakdown step, which can subsequently be switched between a conductive ON state and a less conductive OFF state) with current compliance returned to the low-current state (OFF state) with a sharp decrease in current at approximately +1.5 V (*i.e.*, RESET voltage, V_{RESET}) during the voltage sweep from −2.0 to +2.0 V. After a reversal of voltage polarity, this low-current state was maintained from +2.0 to −1.5 V and then abruptly converted to high-current state at −1.5 V. *Although Ag electrodes were used as top electrodes in these devices, a similar switching behavior was also observed from Au, Pt, or W top electrodes. This indicates that the Ag electrode itself has no significant effect on the resistive switching characteristics of LbL (PAH/ferritin)$_n$ multilayers.*

Acknowledgment. This work was supported by the National Research Foundation (NRF) grant funded by the Korea government (MEST) (2010-0029106; 2010-0027751) and ERC Program of NRF grant funded by the Korea government (MEST) (R11-2005-048-00000-0).

Supporting Information Available: *I*−*V* curve of (PAH/ferritin)$_{15}$, (PAH/PAA)$_{15}$, and (PAH/apoferritin)$_{15}$ multilayers composed of insulating polyelectrolytes and one bare ferritin nanoparticle. This material is available free of charge *via* the Internet at http://pubs.acs.org.

REFERENCES AND NOTES

1. Hoare, R. J.; Harrison, P. M.; Hoy, T. G. Structure of Horse-Spleen Apoferritin at 6 Å Resolution. *Nature* **1975**, *225*, 653–654.
2. Lin, X.; Xie, J.; Zhu, L.; Lee, S.; Niu, G.; Ma, Y.; Kim, K.; Chen, X. Hybrid Ferritin Nanoparticles as Activatable Probes for Tumor Imaging. *Angew. Chem., Int. Ed.* **2011**, *50*, 1569–1572.
3. Lambert, E. M.; Viravaidya, C.; Li, M.; Mann, S. Microemulsion-Mediated Self-Assembly and Silicification of Mesostructured Ferritin Nanocrystals. *Angew. Chem., Int. Ed.* **2010**, *49*, 4100–4103.
4. Kim, K.; Wong, W.; Mann, S. Biomimetic Synthesis of Cadmium Sulfide-Ferritin Nanocomposites. *Adv. Mater.* **1996**, *8*, 928–932.
5. Kasyutich, O.; Ilari, A.; Florillo, A.; Tatchev, D.; Hoell, A.; Ceci, P. Silver Ion Incorporation and Nanoparticle Formation inside the Cavity of *Pyrococcus Furiosus* Ferritin: Structural and Size-Distribution Analyses. *J. Am. Chem. Soc.* **2010**, *132*, 3621–3627.
6. Kwon, M.; Choi, H.; Chang, M.; Jo, M.; Jung, S-J.; Hwang, H. Droplet Evaporation-Induced Ferritin Self-Assembled Monolayer as a Template for Nanocrystal Flash Memory. *Appl. Phys. Lett.* **2007**, *90*, 193512.
7. Qu, X.; Kobayashi, N.; Komatsu, T. Solid Nanotubes Comprising α-Fe_2O_3 Nanoparticles Prepared from Ferritin Protein. *ACS Nano* **2010**, *4*, 1732–1738.
8. Xu, D.; Watt, G. D.; Harb, J. N.; Davis, R. C. Electrical Conductivity of Ferritin Proteins by Conductive AFM. *Nano Lett.* **2005**, *5*, 571–577.
9. Choi, S.; Hong, S.-H.; Cho, S. H.; Park, S.; Park, S.-M.; Kim, O.; Ree, M. High Memory Performance Programmable Memory Devices Based on Hyperbranched Copper Phthalocyanine Polymer Thin Films. *Adv. Mater.* **2008**, *20*, 1766–1711.
10. Ji, Y.; Cho, B.; Song, S.; Kim, T.-W.; Choe, M.; Kahng, Y. H.; Lee, T. Stable Switching Characteristics of Organic Nonvolatile Memory on a Bent Flexible Substrate. *Adv. Mater.* **2010**, *22*, 3071–3075.
11. Bozamo, L. D.; Kean, B. W.; Beinhoff, M.; Carter, K. R.; Rice, P. M.; J. C.; Scott, J. C. Organic Materials and Thin-film structures for Cross-Point Memory Cells Based on Trapping in Metallic Nanoparticles. *Adv. Funct. Mater.* **2005**, *15*, 1933–1939.
12. Son, D. I.; Kim, T. W.; Shim, J. H.; Jung, J. H.; Lee, D. U.; Lee, J. M.; Park, W. I.; Choi, W. K. Flexible Organic Bistable Devices Based on Graphene Embedded in an Insulating Poly(methyl metahcrylate) Polymer Layer. *Nano Lett.* **2010**, *10*, 2441–2447.
13. Decher, G. Fuzzy Nanoassemblies: Toward Layered Polymeric Multicomposites. *Science* **1997**, *277*, 1232–1237.
14. Caruso, F.; Caruso, R. A.; Möhwald, H. Nanoengineering of Inorganic and Hybrid Spheres by Colloidal Templating. *Science* **1998**, *282*, 1111–1114.
15. Lee, B.; Kim, Y.; Lee, S.; Kim, Y. S.; Wang, D.; Cho, J. Layer-by-Layer Growth of Polymer/Quantum Dot Composite Multilayers by Nucleophilic Substitution in Organic Media. *Angew. Chem., Int. Ed.* **2010**, *49*, 359–363.
16. Kim, Y.; Lee, C.; Shim, I.; Cho, J. Nucleophilic Substitution Reaction Based Layer-by-Layer Growth of Superparamagnetic Nanocomposite Films with High Nonvolatile Memory Performance. *Adv. Mater.* **2010**, *22*, 5140–5144.
17. Yoon, M.; Kim, Y.; Cho, J. Multifunctional Colloidal with Optical, Magnetic, and Superhydrophobic Properties Derived from Nucleophilic Substitution-Induced Layer-by-Layer Assembly in Organic Media. *ACS Nano* **2011**, *5*, 5417–5426.
18. Kim, S.; Kim, Y.; Ko, Y.; Cho, J. Electrochemical Sensors Based on Porous Nanocomposite Films with Weak Polyelectrolyte-Stabilized Gold Nanoparticles. *J. Mater. Chem.* **2011**, *21*, 8008–8013.
19. Lee, B.; Kim, Y.; Lee, S.; Kim, Y. S.; Wang, D.; Cho, J. Layer-by-Layer Growth of Polymer/Quantum Dot Composite Multilayers by Nucleophilic Substitution in Organic Media. *Angew. Chem., Int. Ed.* **2010**, *49*, 359–363.
20. Park, J.; Park, J.; Kim, S. H.; Cho, J.; Bang, J. Desalination Membranes from pH-Controlled and Thermally-Cross-linked Layer-by-Layer Assembled Multilayers. *J. Mater. Chem.* **2010**, *20*, 2085–2091.
21. Lee, C.; Kim, I.; Shin, H.; Kim, S.; Cho, J. Nonvolatile Resistive Switching Memory Properties of Thermally Annealed Titania Precursor/Polyelectrolyte Multilayers. *Langmuir* **2009**, *25*, 11276–11281.
22. Lee, J.-S.; Cho, J.; Lee, C.; Kim, I.; Park, J.; Kim, Y.; Shin, H.; Lee, J.; Caruso, F. Layer-by-Layer Assembled Charge Trap Memory Devices with Adjustable Electronic Properties. *Nat. Nanotechnol.* **2007**, *2*, 790–795.
23. Lee, C.; Kim, I.; Shin, H.; Kim, S.; Cho, J. Nonvolatile Memory Properties of Pt Nanoparticle-Embedded TiO_2 Nanocomposite Multilayers via Electrostatic Layer-by-Layer Assembly. *Nanotechnology* **2010**, *21*, 185704–185704.
24. Lee, M. J.; Lee, C. B.; Lee, D.; Lee, S. R.; Chang, M.; Hur, J. H.; Kim, Y. B.; Kim, C.-J.; Seo, D. H.; Seo, S.; *et al.* A Fast, High-Endurance and Scalable Non-volatile Memory Device Made from Asymmetric Ta_2O_{5-x}/TaO_{2-x} Bilayer Structures. *Nat. Mater.* **2011**, *10*, 625–630.
25. Zhang, T.; Su, Z.; Chen, H.; Ding, L.; Zhang, W. Study on Resistance Switching Properties of Sol-Gel Derived $La_{0.67}Ca_{0.33}MnO_3$ Thin Films on F-doped SnO_2 Conducting Glass. *Appl. Phys. Lett.* **2008**, *93*, 172104.
26. Li, G. L.; Liu, G.; Li, M.; Wan, D.; Neoh, K. G.; Kang, E. T. Organo- and Water-Dispersible Graphene Oxide−Polymer Nanosheets for Organic Electronic Memory and Gold Nanocomposites. *J. Phys. Chem. C* **2010**, *114*, 12742–12748.
27. Choi, J.; Rubner, M. F. Influence of the Degree of Ionization on Weak Polyelectrolyte Multilayer Assembly. *Macromolecules* **2005**, *38*, 116–124.
28. Grabar, K. C.; Smith, P. C.; Musick, M. D.; Davis, J. A.; Walter, D. G.; Jackson, M. A.; Guthrie, A. P.; Natan, M. J. Kinetic Control of Interparticle Spacing in Au Colloid-Based Surfaces: Rational Nanometer-Scale Architecture. *J. Am. Chem. Soc.* **1996**, *118*, 1148–1153.
29. Schmitt, J.; Decher, G.; Dressick, W. J.; Brandow, S. L.; Geer, R. E.; Shashidhar, R.; Calvert, J. M. Metal Nanoparticle/Polymer Superlattice Films: Fabrication and Control of Layer Structure. *Adv. Mater.* **1997**, *9*, 61–65.
30. Girardet, J. L.; Blaise, A.; Chappert, J.; Lawrence, J. J.; Feron, J.; Picoche, J. C. Magnetic and Crystallographic Properties of Ferritin. *J. Appl. Phys.* **1970**, *41*, 1002.
31. Tominaga, M.; Soejima, K.; Taniguchi, I. Redox Reaction Characteristics of Ferritin Immobilized onto Poly(L-lysone)-Modified Indium Oxide Electrodes. *J. Electroanal. Chem.* **2008**, *617*, 78–84.
32. Alencar, W. S.; Crespilho, F. N.; Santos, M. R. M. C.; Zucolotto, V.; Oliveira, O. N.; Silva, W. C. Influence of Film Architecture on the

Charge-Transfer Reactions of Metallophthalocyanine Layer-by-Layer Films. *J. Phys. Chem. C* **2007**, *111*, 12817–12821.
33. Tominaga, M.; Soejima, K.; Taniguchi, I. Redox Reaction Characteristics of Ferritin-Immobilized onto Poly(L-lysine)-Modified Indium Oxide Electrodes. *J. Electroanal. Chem.* **2008**, *617*, 78–84.
34. Watt, G. D.; Frankel, R. B.; Papaefthymiou, G. C. Reduction of Mammalian Ferritin. *Proc. Natl. Acad. Sci.* **1985**, *82*, 3640–3643.
35. Liu, X.; Theil, E. C. Ferritins: Dynamic Management of Biological Iron and Oxygen Chemistry. *Acc. Chem. Res.* **2005**, *38*, 167–175.
36. Terabe, K.; Hasegawa, T.; Nakayama, T.; Aono, M. Quantized Conductance Atomic Switch. *Nature* **2005**, *433*, 47–50.
37. Yang, Y. C.; Pan, F.; Liu, Q.; Liu, M.; Zeng, F. Fully Room-Temperature-Fabricated Nonvolatile Resistive Memory for Ultrafast and High-Density Memory Application. *Nano Lett.* **2009**, *9*, 1636–1643.
38. Waser, R.; Aono, M. Nanoionics-Based Resistive Switching Memories. *Nat. Mater.* **2007**, *6*, 833–840.
39. Strukov, D. B.; Snider, G. S.; Stewart, D. R.; Williams, R. S. The Missing Memristor Found. *Nature* **2008**, *453*, 80–83.
40. Yang, J. J.; Pickett, M. D.; Li, X.; Ohlberg, D. A. A.; Stewart, D. R.; Williams, R. S. Memrisitve Switching Mechanism for Metal/Oxide/Metal Nanodevices. *Nat. Nanotechnol.* **2008**, *3*, 429–433.
41. Chudnovskii, F. A.; Odynets, I. I.; Pergament, A. I.; Stefanovich, G. B. Electroforming and Switching in Oxides of Transition Metals: The Role of Metal−Insulator Transition in the Switching Mechanism. *J. Solid State Chem.* **1996**, *122*, 95–99.
42. Waser, R.; Dittmann, R.; Staikov, G.; Szot, K. Redox-Based Resistive Switching Memories-Nanoionic Mechanisms, Prospects, and Challenges. *Adv. Mater.* **2009**, *21*, 2632–2663.
43. Simmons, J. G.; Verderber, R. R. New Conduction and Reversible Memory Phenomena in Thin Insulating Films. *Proc. R. Soc. A* **1967**, *301*, 77–102.
44. Guan, W.; Long, S.; Jia, R.; Liu, M. Nonvolatile Resistive Switching Memory Utilizing Gold Nanocrystals Embedded in Zirconium Oxide. *Appl. Phys. Lett.* **2007**, *91*, 062111.
45. Park, J.-G.; Nam, W.-S.; Seo, S.-H.; Kim, Y.-G.; Oh, Y.-H.; Lee, G.-S.; Paik, U.-G. Multilevel Nonvolatile Small-Molecule Memory Cell Embedded with Ni Nanocrystals Surrounded by a NiO Tunneling Barrier. *Nano Lett.* **2009**, *9*, 1713–1719.
46. Cho, B.; Song, S.; Ji, Y.; Kim, T.-W.; Lee, T. Organic Resistive Memory Devices: Performance Enhancement, Integration, and Advanced Architectures. *Adv. Funct. Mater.* **2011**, *21*, 2806–2829.
47. Leone, A. M.; Weatherly, S. C.; Williams, M. E.; Thorp, H. H.; Murray, R. W. An Ionic Liquid Form of DNA: Redox-Active Molten Salts of Nucleic Acids. *J. Am. Chem. Soc.* **2001**, *123*, 218–222.